2010 IEEE International Conference on Robotics and Automation
Anchorage Convention District
May 3-8, 2010, Anchorage, Alaska, USA

Brake Design for Dynamic Modular Robots

Chris E. Thorne, Nikita Skorodinski, Hughes Tipton, Travis Van Schoyck, Mark Yim

Abstract— **An energy efficient joint-locking mechanism that works in conjunction with the main actuator of a robot module is presented. The mechanism will enable chain-style modular reconfigurable robots to perform a wide array of tasks such as dynamic motion and bio-inspired locomotion while consuming less power. The design process for developing this mechanism is presented, and analysis is provided. This mechanism is ideal for modular reconfigurable robot systems, but can be modified to suit many applications. A prototype is developed that outperforms comparable devices such as those that utilize piezoelectrics, magnetic particles, and electromagnetically-actuated disc and drum brakes in terms of power consumption and specific torque.**

I. INTRODUCTION

Modular reconfigurable robots are systems comprised of many simple repeated units called modules[1][2][4][5][7][9]. These modules typically have one or two *degrees-of-freedom* (*DOF*) and can be connected in multiple ways to suit a given task.

There are two competing factors towards maximizing capability of these systems: *specific torque* (motor torque per module mass) and *power consumption*. Larger torque typically requires more mass and, in turn, more power for actuation. In addition smaller modules lead to shorter lever arms (larger mechanical advantage) and typically lower mass. Therefore considerable efforts have been made in the modular reconfigurable robot community to reduce size of the component modules [13].

Locking a joint allows modules to passively hold a configuration with much larger holding torque than with a joint actuator. A typical chain-style modular robot, like the Connector Kinetic Robot *(CKbot)* developed in the *Modlab*, may have dozens of active modules in a given configuration. The system correspondingly has dozens of *DOF*.

In this work, we propose a design for a joint-locking device *(brake)* for modular robots using the axiomatic design process [11] – a powerful tool that can be used systematically to develop solutions to many design problems. The brake is electro-magnetically actuated. It is bistable, consuming no power to maintain a torque, and has better *specific torque* than the low power magnetic particle, piezoelectric transducer (PZT)-based and the electro-magnetic disc brakes. It will be incorporated into a new single *DOF* module that is actuated by a direct-drive brushless outrunner motor. The addition of this component will enable various advances: (1) executing kinodynamic motion plans that are currently hindered by the use of highly-geared position controlled servos, as in [10], where modular robot systems take advantage of inertia to achieve otherwise unobtainable configurations. (2) locking joints to create bone type structures that enable high mechanical advantage in parallel and lever-like configurations [14]. (3) developing bio-inspired control where modules can push and pull against other modules acting as bone structures that consume no power [3]. (4) enabling longer battery life for remote untethered tasks by alleviating the burden on the joint actuator when required to maintain a state.

The authors are with the department of Mechanical Engineering and Applied Mechanics, University of Pennsylvania, Philadelphia, PA, USA. Contact: ecthorne@seas.upenn.edu;

A. Related Work

There is a variety of commercially available brakes including those based on electromechanical actuation, magnetic particle brakes, and PZT brakes. Electromagnetic disc brakes are common and can apply large holding torques relatively fast without excessive size and weight. The magnetic particle brakes and PZT brakes consume much less power and can have large bandwidth, but tend to be large with poor *specific torque*.

Numerous brake designs have been used in robotic systems. Traditional electromagnetic brakes are common in light-weight robot arms [8], though these brakes are too large and too heavy for typical modular robot systems. In [6], a PZT-actuated drum brake prototype that utilizes a compliant mechanism to amplify the displacement is presented. Some systems use transmissions that are not backdrivable to obtain similar functionality. In [12], the I-Cubes are a heterogeneous group of modules with *3-DOF* bars and passive nodes. They use worm gears and servos for actuation. Worm gears are naturally self-locking at the expense of speed and cannot exploit dynamic motions (motions in which inertia play a significant role).

B. Axiomatic Design Overview

The axiomatic design process provides a method for applying structure, common language, and metrics to design to enable quantitative comparison and evaluation. In this paradigm, designs are represented as a collection of functional requirements (*FRs*) and design parameters (*DPs*). The *FRs* are the minimum set of independent design goals and are elements of the functional space, while the *DPs* represent the physical means to satisfy those *FRs* and reside in the physical space. Both *FRs* and *DPs* are organized in hierarchies, starting from the most fundamental goal of the design down to the smallest subsystem. Constraints (*Cs*) may apply to the entire hierarchy or be present at some levels due to the choice of *DPs* in previous levels. *FRs*, *DPs*, and *Cs* are organized within the hierarchy with subscripts; FR_{ij}, where i indicates the hierarchy level and j the location within the hierarchy.

II. DESIGN DECOMPOSITION

The joint-locking mechanism design is decomposed into a hierarchy of *FRs* and *DPs*, shown in Figure 1, where each

block in the *FR* hierarchy has a corresponding block in the *DP* hierarchy.

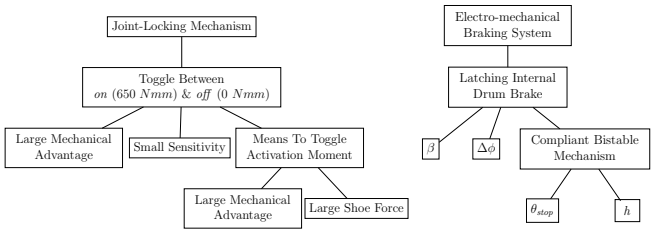

Fig. 1. *(left) FR* and, *(right) DP* hierarchies

A. System Constraints

Several constraints apply to the system as a whole and must be enforced at every level of the hierarchy. These constraints are denoted ${}^{sys}C_i$. The system constraint ${}^{sys}C_1$ represents the need to fit the brake in the internal space of the module with the main actuator. We desire large specific torque (${}^{sys}C_2$) to keep the modules as light as possible. Less brake mass results in an overall decrease in module mass and a smaller required holding torque from the brake. We also require that the mechanism has identical performance for both clockwise and counterclockwise motion of the main actuator (${}^{sys}C_3$).

TABLE I

SYSTEM CONSTRAINTS

${}^{sys}C_1$ = Occupy less than half the volume ($\leq 55\ cm^3$)
${}^{sys}C_2$ = Low mass (large specific torque) ($\leq 45\ grams$)
${}^{sys}C_3$ = Performance independent of direction

B. Level 1

The highest level of the hierarchy describes the overarching goal for the mechanism: resist motion of a module's joint up to some maximum applied torque. As a benchmark, we consider five modules rigidly connected in a chain cantilevered horizontally to a wall. Assuming ${}^{sys}C_2$ is satisfied and the new direct-drive module has comparable mass to the existing *CKbot* module, the required joint locking moment is approximately 600 *Nmm*. In addition, for the brake to be practical on a modular robot, it must require minimal energy to operate, as modules are typically battery powered.

TABLE II

HIERARCHY LEVEL 1: JOINT LOCKING SYSTEM

FR_{11} = Low energy joint-locking mechanism with holding torque $\geq$ 600 *Nmm*
DP_{11} = Capacitive electro-mechanical braking system

The brake's ability to store energy as in [6] is desirable. Some systems that may satisfy FR_{11} include drum, band, cone, disk, hysteresis and magnetic particle brakes. Brakes that rely on phenomena such as eddy-currents, however, do not satisfy the requirements because they cannot provide torque at zero velocity.

C. Level 2

The *FR* in the second level of the hierarchy further specifies a means for low energy operation.

TABLE III

HIERARCHY LEVEL 2: ELECTRO-MECHANICAL BRAKING SYSTEM

FR_{21} = Toggle between passively stable *on* & *off* states
DP_{21} = Latching internal drum brake

A latching internal drum brake is a good candidate for the braking system based on the functional requirement listed in Table III and on the system constraints. Cone brakes have similar performance to drum brakes, but are harder to fit within a given space. Externally pivoted shoe and band brakes are effective, but, since space is limited (${}^{sys}C_1$), they will typically result in less *specific torque*. Magnetic particle brakes and hysteresis brakes require energy to maintain braking torque and thus violate FR_{21}. Disk brakes have no friction moment (discussed in II-D) and thus require a large activation force compared to drum or cone brakes, typically resulting in lower *specific torque*. A latching internal drum brake (*e.g.* an emergency brake in an automobile), satisfies both the functional requirements and the system constraints.

D. Level 3

Direction independent performance (${}^{sys}C_3$) requires two shoes in the internal pivoted drum brake. A bistable mechanism allows both shoes to be toggled between the *on* and *off* states without requiring energy to remain in either state. A Matlab model provides a means of estimating the elements of the design matrix.

We construct the model by first considering a single shoe contacting the drum as in Figure 2. Assuming a rigid shoe and drum, linearly elastic brake lining, and negligible pressure variation through the width of the brake, we express the pressure along the lining due to an incremental rotation, $\delta\alpha$, about the pivot as

$$p = Kr\delta\alpha sin\phi \tag{1}$$

where K is an unknown constant, r is the radius to the shoe pivot and ϕ is the angle to a lining element measured from the line connecting the center of the drum with the pivot, denoted ϕ_{ref}. The equation can be simplified further by noting that the pressure is a maximum at p_{max}, when $sin\phi$ is maximum. We can rewrite equation 1 as

$$p = \frac{p_{max}}{(sin\phi)_{max}} sin\phi \tag{2}$$

The pressure variation along the brake lining gives rise to both pressure and friction induced moments about the pivot. We find these moments by integrating the incremental friction and normal forces along the lining

$$\begin{aligned} M_p &= \frac{rF_{max}}{4}(2\Delta\phi - sin2\phi_2 + sin2\phi_1) \\ M_f &= \frac{\mu F_{max}}{4}[4R(cos\phi_1 - cos\phi_2) - r(cos2\phi_1 - cos2\phi_2)] \end{aligned} \tag{3}$$

where F_{max} is defined as follows

$$F_{max} = \frac{Rwp_{max}}{(sin\phi)_{max}} \tag{4}$$

where R is the drum inner radius, w is the shoe width (into the page), and ϕ_1 and ϕ_2 are the angles to the lower and upper extents of the lining as measured from ϕ_{ref} respectively, as shown in Figure 2. $\Delta\phi$ is the angular range of the lining and is calculated from $\Delta\phi = \phi_2 - \phi_1$. The activation moment, M_a, is the sum of the pressure moment and the friction moment about the pivot. We find the braking torque in a similar manner by integrating the incremental friction force along the lining:

$$\tau = \frac{\mu R^2 wp_{max}}{(sin\phi)_{max}}(cos\phi_1 - cos\phi_2) \tag{5}$$

Equations *3* through *5* relate the desired holding torque to the activation moment on the shoe. If the direction of rotation is toward a shoe's pivot, the shoe is called a leading shoe and tends to pull into the drum. Conversely, if the direction of rotation is away from a shoe's pivot, the shoe is called a trailing shoe and tends to pull away from the drum. For a given direction of drum rotation, one shoe leads and the other shoe trails. When the same activation moment is applied to both shoes, the leading shoe contributes more to the overall braking torque, as illustrated in Figure 3.

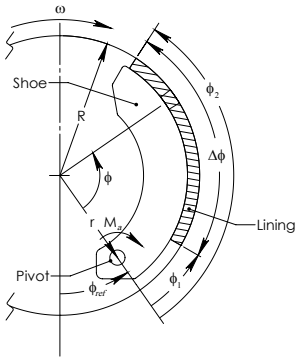

Fig. 2. Pivoted internal drum brake

The parameters used in the Matlab model of the drum brake are: $\beta = r/R$, the non-dimensional pivot radius; μ, the static coefficient of friction between the shoe and the drum, w, ϕ_1, ϕ_{ref} and $\Delta\phi$. μ is constrained by the choice of available lining materials. w should be as large as possible to maximize mechanical advantage without violating the system constraints. ϕ_{ref} shifts the lining and is only of interest in the final mechanical design to prevent the shoes from interfering. ϕ_1 is small for large values of $\Delta\phi$ and has an optimum value that maximizes equation 5 given $\Delta\phi$. The parameters β and $\Delta\phi$ prove to have sufficient freedom to be used as the first two *DPs* at this level of the hierarchy.

TABLE IV

HIERARCHY LEVEL 3: PIVOTED INTERNAL TWO-SHOE DRUM BRAKE

FR_{31} = Large mechanical advantage, $\eta = \tau_{out}/(M_f + M_p)$
FR_{32} = Low sensitivity, $S \leq 2$
FR_{33} = Means to toggle activation moment
C_{31} = Self-locking parameter, $SL \leq 1$
C_{32} = Maximum pad pressure, $P_{max} \leq 1$ *MPa*
DP_{31} = Nondimensional pivot radius, β
DP_{32} = Lining span, $\Delta\phi$
DP_{33} = Compliant bistable mechanism

Mechanical advantage (η), FR_{31}, is defined here as the ratio of the output static holding torque of the brake to the total activation moment on the shoes. Sensitivity (S), FR_{32}, is a non-dimensional quantity that measures the variation of braking torque with friction coefficient at fixed activation moment. Sensitivity values less than 2 are considered appropriate for well behaved brakes. A Matlab model generates reaction force diagrams as in Figure 3 which provides information on how the various components are loaded.

The *DPs*, β and $\Delta\phi$, are limited to a subsection of their full ranges: β may vary between 0.625 and 0.9 to accommodate internal components, and $\Delta\phi$ may vary between 25° and 100° to prevent interference between the two shoes. The *DPs* are normalized in this range to enable comparison of their

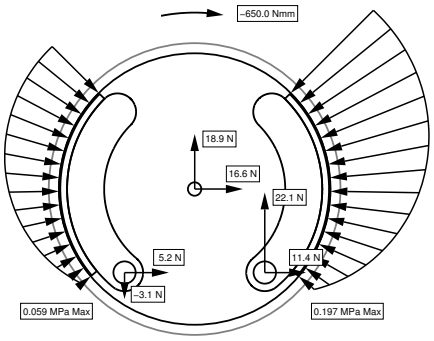

Fig. 3. Matlab model reaction force diagram

individual contributions. A tilde, $\widetilde{\{\}}$, indicates normalized parameters. Several parameters that characterize the performance of the drum brake must be evaluated in order to check constraints. Self-locking (*SL*), C_{31}, indicates that M_f dominates M_p, resulting in drastically reduced control. *SL* is defined as the ratio of the friction moment to the pressure moment and is required to be between -1 and 1.

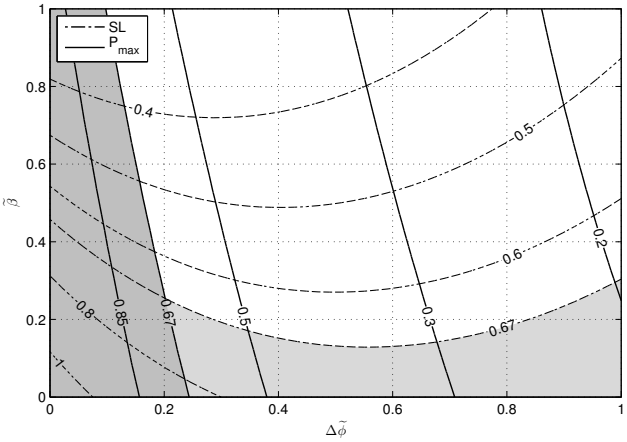

Fig. 4. Drum brake *C* isograms plotted in the design space: self-locking parameter, *SL* and maximum lining pressure, P_{max} (*MPa*). Shaded areas denote the factor of safety violation.

The maximum lining pressure (P_{max}), C_{32}, is dictated by the lining material specification. 1 *MPa* in our case. We use a factor of safety of 1.5 for the *SL* and P_{max} constraints. Figure 4 shows contours of the two constraints as a function of the two normalized *DPs*. The shaded regions indicate where *Cs* are violated. As the Figure confirms, much of the design space is still available.

The general form of the design equation, discussed in section I-B, is

$$\{FR\} = [A]\{\widetilde{DP}\}, \text{with } \{FR\} = \begin{bmatrix}\eta \\ S\end{bmatrix}, \{\widetilde{DP}\} = \begin{bmatrix}\widetilde{\beta} \\ \Delta\widetilde{\phi}\end{bmatrix} \quad (6)$$

The relationships between the *DPs* and *FRs* are shown in Figures 5. Both *FRs* vary nonlinearly with both *DPs* so the Jacobian of the design equation must be found in order to make the system linear. This is the tangent design space at a point of interest. We must choose a point to linearize about that satisfies the constraints, the *FRs* and that results in a manageable degree of coupling. One such point is $(\Delta\widetilde{\phi}, \widetilde{\beta}) = (0.76, 0.63)$. At this point, η is 1.2 and S is 1.68 which corresponds to a required shoe force of 14.89 N. The Jacobian ($[A]$ matrix) at this point is represented in Figure 5

by the two tangent planes and is calculated as

$$[A] = \begin{bmatrix} -0.92 & -0.11 \\ -1.13 & 0.9 \end{bmatrix} \quad (7)$$

Since only the *DPs* are normalized, the elements in the design matrix can only be compared column-wise for their contributions to the respective *FR*. We consider equation 6 with the *FRs* and *DPs* calculated with respect to the point at which the design equation is normalized. Noting that the contribution of $\widetilde{\Delta\phi}$ to η in this neighborhood is small compared to the $\widetilde{\beta}$ contribution, the A_{12} element of the design matrix can be neglected, yielding a decoupled design. This approximation was calculated more formally through the use of coupling metrics as in [11], not included here for length. It is worth noting that there are other points in the design space that also yield locally decoupled designs.

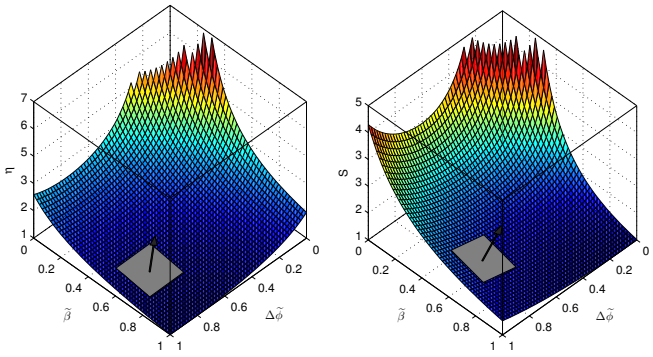

Fig. 5. *(left)* Drum brake mechanical advantage, η (FR_{31}) and *(right)* sensitivity, S (FR_{32}), as a function of pivot radius, $\widetilde{\beta}$ and lining range, $\Delta\widetilde{\phi}$

E. Level 4

A compliant bistable mechanism satisfies DP_{33} due to its superior qualities over conventional rigid-linked mechanism: no joint friction, ability to be manufactured as a monolithic part, and no joint play, resulting in higher precision. We choose a compliant mechanism design that can be modeled as a slider-crank inversion. It incorporates a living hinge between the crank and the slider, which itself is an initially-curved beam that acts as a linear spring. This mechanism has two stable states that are symmetric about the horizontal, where the mechanism is unstable. The *3-D* model and the mechanism's pseudo-rigid-body model are shown in Figure 6. A hard stop is placed at a crank angle less than the stable crank angle to provide a non-zero shoe force at one of the stable states.

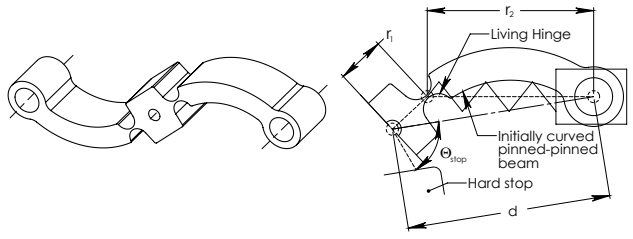

Fig. 6. Compliant bistable mechanism *(left)* 3-D model and *(right)* pseudo-rigid-body model (half model shown)

The crank, r_1, is assumed to be rigid, and the living hinge is assumed to operate like an ideal pin joint. The equations that describe the force-deflection characteristics of initially curved beams are well known in the literature and are not repeated here.

TABLE V

HIERARCHY LEVEL 4: COMPLIANT BISTABLE MECHANISM

FR_{41} = Mechanical advantage, $\eta \geq 2\ mm^{-1}$
FR_{42} = Shoe Force, $F_{shoe} \geq 14.89\ N$
C_{41} = Contained inside drum: $R \leq 26\ mm$, $w \leq 6\ mm$
C_{42} = Factor of safety, $FS \geq 3$
C_{43} = Output force sensitivity, σ to variations in ground link length (d), $\geq -250\ N/mm$
C_{44} = Torque input from hobby brushless outrunner motor *(Mighty Midget)*, maximum continuous output torque, $\tau_{max} = 36\ Nmm$
DP_{41} = Non-dimensional hard stop offset angle, $\widetilde{\theta}_{stop}$
DP_{42} = Non-dimensional beam thickness, $\widetilde{h}$

The bistable mechanism must use the supplied actuation moment to toggle a force on the shoes between 0 N and 14.98 N. Two *FRs* can be defined to encapsulate this goal, namely mechanical advantage, η (FR_{41}), which is defined as the ratio of the output force at the hard stop angle, θ_{stop}, to the maximum crank torque through the mechanism's range of motion, and shoe force, F_{shoe} (FR_{42}), which is the output force at the hard stop.

θ_{stop} is a natural choice for DP_{41} because it enables the adjustment of the output force without affecting the maximum crank torque. h allows adjustment of both the shoe force and crank torque, making it a good choice for DP_{42}.

There are many choices for driving the compliant bistable mechanism. Shape memory alloy (*SMA*) wires are attractive because they have low mass and can generate large forces, however, the cooling time required makes them too slow. Piezoelectric actuation requires a large gain on the displacement making it difficult to use at this scale. Electromagnets generally have poor *specific torque*, and pneumatics would require a bulky supply tank on the module. Small DC brushless (*BLDC*) outrunner motors have good *specific torque* and are readily available in small form factors in the hobby market. The *Mighty Midget* is a BLDC that can continuously supply 36 *Nmm* of torque without a gear train and has a mass of 6.5 *grams*. The selection of this motor, coupled with the shoe force required from the results of the previous level of the hierarchy gives a target value for FR_{41}.

In addition to the size constraints, there are operational constraints on the mechanism that depend on h: output sensitivity, σ (C_{43}) and factor of safety, FS (C_{42}). σ is the initial rate at which F_{shoe} decreases as the distance between the crank shaft and shoe pin increases due to lining wear and joint play. FS indicates how close the maximum stress in the curved beam gets to the endurance limit given the prescribed cyclic loading.

As with the subsystem in *level 3* of the hierarchy, the compliant bistable mechanism has a nonlinear design equation that can be linearized at a nominal point in the design space. This can then be combined with the results from equation 6 to obtain a system design equation.

III. PROTOTYPE

The prototype consists of a frame and a rotating counterweight assembly. Figure 7 shows a cutaway view of the prototype detailing the drum, shoes, and compliant bistable mechanism.

A hobby brushless outrunner motor drives the main *DOF* of the prototype. This motor simulates the module *DOF* and is mounted to one of the two frame plates. The counterweight assembly is comprised of the brushless outrunner rotor, the brake drum, and a lever arm that supports an adjustable counterweight. The motor shaft protrudes through the lever arm and drum, and is supported by a ball bearing in the other frame plate. The lever arm and counterweight approximate the effect of a collection of four CKbot modules. The two brake shoes rotate on dual ball bearings about precision shoulder screw pivots. Ferotec Friction Flexible Molded Material model number D-4080 provides the friction material or brake lining on the shoes due to its favorable compressibility rating and static friction coefficient of 0.65.The *Mighty Midget BLDC* is mounted in a recessed portion of one of the frame plates. This motor connects to the crank of the compliant bistable mechanism to toggle it between the *on* and *off* states. A microcontroller and magnetic encoders are used to commute and perform control for both brushless motors.

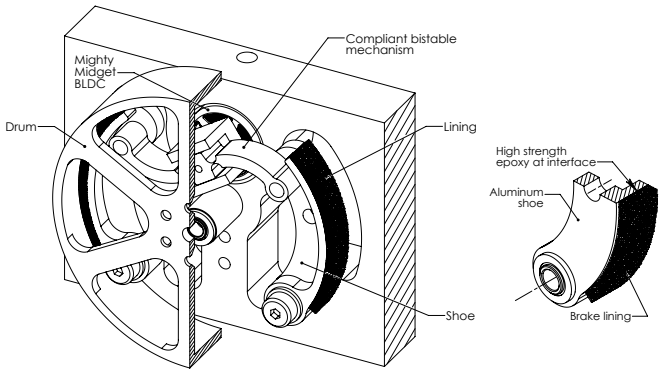

Fig. 7. *(left)* Prototype assembly interior cutaway exposing the shoes and compliant bistable mechanism and *(right)* Shoe and brake lining

IV. Performance

Several experiments were performed to evaluate the performance of the proposed brake design. First, the static load capability of the brake was tested by checking its ability to hold various counterweights in the horizontally extended position. The brake is capable of producing a maximum of *480 Nmm* of static holding torque which falls short of the intended *600 Nmm*. This discrepancy is due primarily to manufacturing tolerances and the lack of full surface contact at the lining-drum interface. The compliant bistable mechanism attaches to the shoes through a pin joint comprised of a steel pin and a carefully machined hole. This joint contributes non-ideal effects such as friction and joint play. These effects reduce the effective available torque from the *Mighty Midget* and result in a larger effective hard stop angle. The reduced surface contact between the drum and the lining is caused almost exclusively by the shoe assemblies since the drum is precision machined with a 16 RMS finish. The linings, however, exhibit surface variations most likely due to uneven pressure applied by the fixture when epoxying the lining to the shoe, as well as inherent thickness variations throughout the lining itself. Over time it is expected that the surface contact will increase as the lining wears and takes on the shape of the drum - typically known as the breaking-in period.

As the brake may be used in systems that incorporate dynamic planning, the second experiment involves the repeatability of the brake. We refer to repeatability as the ability to generate a predetermined braking torque that can be used to plan dynamic motions. To test this, the counterweight assembly was repeatedly released from one of four locations and the brake was triggered at the same point in the swing each time. The four locations were ± 90 and ± 180. The brake was triggered at zero degrees measured from the negative y-axis. The angular displacement is measured from the point at which the brake is triggered to the point that the counterweight assembly comes to rest. The data shows a slight asymmetry with direction due to the differences in the lining discussed above. Assuming the angular displacements are normal, the *95%* confidence intervals for the angular displacement standard deviations are computed for each of the four release cases, the worst of which is $[0.81, 2.03]$ *degrees*. This is a reasonable amount of uncertainty and can be accounted for in planning tasks.

Although the brake's primary function is to provide static holding torque, it is also desirable to test the brakes dynamic performance. An experiment similar to the repeatability was conducted but with much higher temporal resolution. In this experiment, the counterweight assembly was released from the vertical and the brake was again triggered at zero degrees (straight down). Figure 8 shows the angular displacement of the counterweight assembly from the point at which the brake is triggered for releases on both sides. A dynamic model of the pendulum was fit to the experimental data in order to solve for the average braking torque. The angular displacement predictions of the model are shown for torques of *585 Nmm* and *663 Nmm* for the left and right releases respectively. As in the repeatability data, there is asymmetry with respect to the direction of motion. It should also be noted that the average braking torque here is slightly larger than the static holding torque despite the fact that the kinetic coefficient of friction is typically smaller than the static one. This increase occurs because the bistable mechanism passes through a singularity as it toggles and exerts a larger shoe force than the designed value at the hard stop.

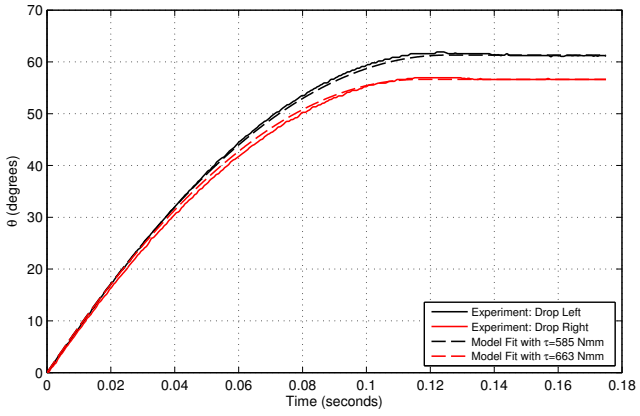

Fig. 8. Angular displacement, vertical release both directions, brake triggered at zero degrees.

A comparison of the new prototype with commercially available brake systems is listed in Table VI along with one

PZT brake prototype [6]. The FB11 is a small electromagnetic brake made by *Inertia Dynamics*. 14.110.04 is another electromagnetic brake made by *magneta GmBH & Co*. The B2 is a magnetic particle brake made by Placid Industries.

The performance characteristics considered are the physical dimensions, the power required to maintain the maximum static torque, the engagement time t_e, the mass, and the static torque τ. All of these values were taken from data sheets or publications. The CKbot brake was tested experimentally and the numbers listed were determined for the maximum counterweight.

TABLE VI
PERFORMANCE COMPARISON

Brake	Dim. *(cm)*	P *(W)*	t_e *(s)*	Mass *(g)*	τ *(Nmm)*
FB11	3.2×3.2×2.5	5.4		91	677
14.110.04	2.2×2.2×3.7	8	0.03	177	2200
B2 MPB	5.3×5.3×3.0	0.25	0.1	450	280
PZT	7.1×7.1×3.8	0	0.003	560	180
CKbot	6.3×6.2×1.1	0	0.0124	40	480

The mass of the CKbot brake prototype is 40.5 *grams* – by far the lightest of the group. The static holding torque is 480 *Nmm*. This results in a specific torque for the brake of 11.85 Nmm/g, compared to a specific torque of 12.43 *Nmm/g* for the 14.110.04, 7.45 *Nmm/g* for the FB11, 0.62 *Nmm/g* for the B2 and 0.32 *Nmm/g* for the PZT-actuated drum brake.

While the largest dimension of the brake is more than double that of the electromagnetic disc brakes, the smallest dimension is less than half. This flat profile works better for the modular robots as the brake can be accommodated in a layered fashion into the module along the shaft of a main actuator.

The electromagnetic brakes show slightly better *specific torque* and smaller size but they consume large amounts of power even when static. The magnetic particle and PZT brakes consume much less power, though their specific torque is much worse, and they are larger.

Despite having a moderate *specific torque*, the PZT brake has advantages such as very large bandwidth with typical activation times on the order of a few milliseconds and the ability to keep the brake engaged without requiring energy.

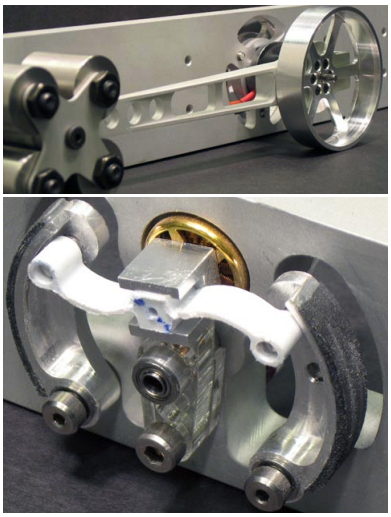

Fig. 9. Prototype *(top)* counterweight assembly and *(bottom)* shoes and compliant bistable mechanism

V. CONCLUSION

In this work, the design of a brake is presented that will enable the next generation of modular robots to execute dynamic motion plans, achieve high mechanical advantage configurations, utilize bio-inspired control, all with longer battery life. The axiomatic design approach has been shown to be a useful tool in designing such systems. A prototype of the brake was demonstrated and its performance compared to both commercially available braking systems and comparable research prototypes. Future work will consist of increasing the static holding torque and integrating the brake into a new modular robot design that is capable of a wide range of dynamic actions.

VI. ACKNOWLEDGEMENTS

The authors acknowledge Peter Szczesniak, William Price, and Amy Fantasia for their input and expertise.

REFERENCES

[1] H.C.H. Chiu, M. Rubenstein, and W.M. Shen. Multifunctional SuperBot with Rolling Track Configuration. In *IROS 2007 Workshop on Self-Reconfigurable Robots & Systems and Applications*, pages 50–53, 2007.

[2] D. J. Christensen and K. Stoy. Selecting a meta-module to shape-change the ATRON self-reconfigurable robot. In *Proceedings of IEEE/RSJ International Conference Robotics and Automation*, pages 2532–2538, Orlando, 2006.

[3] D.J. Christensen, D. Brandt, and K. Stoy. Towards artificial ATRON animals: scalable anatomy for self-reconfigurable robots. In *Proceedings of the Robotics Science and Systems: Workshop on Self-Reconfigurable Modular Robots*, 2006.

[4] D. Duff, M. Yim, and K. Roufas. Evolution of polybot: A modular reconfigurable robot. In *Proc. of the Harmonic Drive Intl. Symposium, Nagano, Japan, Nov*. Citeseer, 2001.

[5] T. Fukuda and S. Nakagawa. Dynamically reconfigurable robotic system. In *Proceedings of IEEE/RSJ International Conference Robotics and Automation*, volume 3, pages 1581–1586, 1988.

[6] M. Gogola and M. Goldfarb. Design of a PZT-actuated proportional drum brake. *IEEE/ASME transactions on mechatronics*, 4(4):409–416, 1999.

[7] R. Groß and M. Dorigo. Fifty years of self-assembly experimentation. In *Workshop and Tutorials – CD, 2007 IEEE/RSJ Int. Conf. on Intelligent Robots and Systems (IROS); Self-Reconfigurable Robots/Systems and Applications Workshop*, pages 21–26. San Diego, CA, 2007.

[8] G. Hirzinger, A. Albu-Schaffer, M. Hahnle, I. Schaefer, and N. Sporer. On a new generation of torque controlled light-weight robots. In *IEEE International Conference on Robotics and Automation*, volume 4, pages 3356–3363. IEEE; 1999, 2001.

[9] K. Hosokawa, I. Shimoyama, and H. Miura. Two-dimensional micro-self-assembly using the surface tension of water. *Micro Electro Mechanical Systems, 1996, MEMS '96, Proceedings. 'An Investigation of Micro Structures, Sensors, Actuators, Machines and Systems'. IEEE, The Ninth Annual International Workshop on*, pages 67–72, Feb 1996.

[10] Ioan Alexandru Sucan, Jonathan F. Kruse, Mark Yim, and Lydia E. Kavraki. Kinodynamic motion planning with hardware demonstrations. In *IEEE/RSJ International Conference on Intelligent Robots and Systems*, pages 1661–1666, Nice, France, 2008.

[11] N.P. Suh. *The principles of design*. Oxford University Press, USA, 1990.

[12] C. Unsal and PK Khosla. Mechatronic design of a modular self-reconfiguring robotic system. In *IEEE International Conference on Robotics and Automation, 2000. Proceedings. ICRA'00*, volume 2, 2000.

[13] P. J. White and M. Yim. Scalable modular self-reconfigurable robots using external actuation. In *Proceedings of IEEE/RSJ International Conference on Intelligent Robots and Systems*, pages 2773–2778, San Diego, 2007.

[14] M. Yim, D. Duff, and Y. Zhang. Closed chain motion with large mechanical advantage. In *Proc. of the IEEE/RSJ Intl. Conf. on Intelligent Robots and Systems*, 2001.